

# Stability of coupled solitary wave in biomembranes and nerves

G. Fongang Achu and F. M. Moukam Kakmeni\*

*Complex Systems and Theoretical Biology Group (CoSTBiG),*

*Laboratory of Research on Advanced Materials and Nonlinear Science (LaRAMaNS),*

*Department of Physics, Faculty of Science, University of Buea, PO Box 63, Buea, Cameroon*

(Dated: February 4, 2022)

In this work, we consider the electromechanical density pulse as a coupled solitary waves represented by a longitudinal compression wave and an out-of-plane transversal wave (i.e., perpendicular to the membrane surface). We analyzed using, the variational approach, the characteristics of the coupled solitary waves in the presence of damping within the framework of coupled nonlinear Burger-Korteweg-de Vries-Benjamin-Bona-Mahony (BKdV-BBM) equation. It is shown that, the inertia parameter increases the stability of coupled solitary waves while the damping parameter decreases it. Moreover, the presence of damping term induces a discontinuity of stable regions in the inertia-speed parameter space, appearing in the form of an island of points. Bell shape and solitary-shock like wave profiles were obtained by varying the propagation speed and their linear stability spectrum computed. It is shown that bell shape solitary wave exhibit bound state eigenvalue spectrum, therefore stable. On the other hand, the solitary-shock like wave profiles exhibit unbound state eigenvalue spectrum and are therefore generally unstable.

## I. INTRODUCTION

Nerve cells are encapsulated by a plasma membrane; a thin quasi-two-dimensional layer consisting mainly of lipids and proteins. Lipid membrane is integral parts of every living cell; attributing an important role in signaling integration to the lipid membrane. They have been reported to resist pressure, stretching, tension, and bending. It has been proposed that these perturbations, in the form of a density or voltage pulses, may play a major role in inter or intracellular communications [1–3] as well as nerve pulse propagations [4, 5]. Signal transduction across the plasma membrane via various receptors and ion channels has received much attention. In a now-classic model proposed by Hodgkin and Huxley, the ionic hypothesis is used to explain the generation and propagation of action potential. According to the ionic hypothesis, voltage-gated ions channels are seen as being responsible for action potential propagation along the plasma membrane of the neuronal axon [6–8]. The Hodgkin-Huxley model is an electrical model based on two conductors (cytosol and extracellular space) separated by a capacitor (plasma membrane) with ions specific channels (proteins). This model is the currently accepted model, substantiated by the discovery of ion channels [9] and their crystallization [10]. However, the ionic hypothesis has been unable to explain the non-electric phenomena observed during the propagation of action potential: swelling of the axon, phase transition, shortening of the axon, and adiabatic nature of action potential. A thermodynamic theory was therefore proposed by Heimburg and Jackson in 2005 to address some these issues [4]. A thermodynamic or soliton theory of nerve pulse propagation hypothesizes that the action potential propagates

in the form of a soliton, or sound wave, along with the lipid bilayer [1, 2, 4, 11]. According to this theory, the compression of a lipid membrane will change its density resulting to phase transitions from a liquid state to a gel state accompanied by the propagation of a density pulse in the gel state. Thus in the soliton theory, the transmission, storage, and information processing are intrinsic properties of the lipid bilayer. The soliton model is based on the propagation of a localized density wave in the axonal membrane [4, 5]. The important requirement of the model is the empirically known lipid phase transitions slightly below the physiological temperatures. The soliton model has been successful in predicting the exact pulse propagation velocities in myelinated nerves. The propagation velocities are closely related to the lateral sound velocities in the nerve membrane [4, 5]. Moreover, the soliton model explains the reversible temperature and heat exchanges observed in connection with the nerve pulse. In the soliton theory, the appearance of a voltage pulse is explained to be a consequence of the piezoelectric nature of partially charged and asymmetric cell membrane [4, 5].

A great effort is being devoted to the deciphering of the mechanism of signal propagation in the axon, in particular, the coupling between electrical and mechanical waves in the form of the longitudinal compression waves [1–5, 11–19]. Sound propagates well in lipid membranes in the form of the longitudinal compression wave. What is not is not obvious, though, is whether the out-of-plane transversal mode can propagates in disordered systems such as biomembrane and nerves. Many experiments have been carried out to detect transverse wave propagation in the lipid membrane. As early as 1988, Vogel and Möbius investigated surface density fluctuations in lipid monolayers at air/water interfaces by superposing two transverse capillary waves under resonance such that their two wave vectors are orthogonal [20]. They

---

\* Corresponding Author, Email: moukamkakmeni@gmail.com

observed that the surface density fluctuations propagate longitudinally along the lipid monolayers. In addition, the wavelength of the transverse mode of the transverse capillary waves was found to be modulated by the longitudinal waves at resonance. This results clearly indicate the inherent coupling between the longitudinal and the transverse mode. In the soliton theory for the action potential, a two-dimensional sound wave propagates along the membrane plane, described by lateral compressibility and a correlated change in density. When applied to the axon, the action potential is considered as a one-dimensional represented by a longitudinal compression pulse since the diameter of the axon is assumed to be smaller than the length of the nerve pulse [4, 13–19]. In contrast, El Hardy and Machta consider not only the longitudinal compressional dislocations but also an out-of-plane transversal mode (i.e., perpendicular to the membrane surface) that Heimburg and Jackson did not consider. This means that El Hardy and Machta effectively consider a three-dimensional wave propagation along the axon. That is, two in a plane and one out of a plane and assuming the axon to display a circular cross-section as in the case of the soliton model, they get rid of one dimension [21]. Thus, the electromechanical density pulses in the nerve can effectively be considered as a vector soliton with two components. That is, the longitudinal component corresponding relative height field, and the transverse components corresponding to lateral stretch field, and have been observed during nerve pulse propagation in garfish olfactory nerve, squid giant axon, and hippocampal neuron [21].

Stimulation of peripheral nerves can be used for the treatment of the dysfunction of the lower urinary tract, chronic pain, epilepsy, and other neurological disorders [22]. It is worth noting in this connection that the composition of the phospholipid bilayer of neurons in terms of its constitutive lipid has been strongly implicated in the the onset of neurobiological and psychiatric disorders [23]. It will be of great interest to understand the characteristics of signal propagation in a lipid bilayer; a “device” for memory storage and information processing, as it might play a role in the functional success of neurotherapy. As a consequence, a right mathematical model of pulse propagation in the lipid membrane and nerve is therefore required. In this work, we have considered the coupled solitary wave model for action potential derived from the improved soliton model of nerve. We investigated in section II, using the variational approach the characteristics of a coupled solitary waves in the presence of damping within the framework of coupled nonlinear Burger-Korteweg-de Vries-Benjamin-Bona-Mahony equations (BKdV-BBM) derived from the vector Boussinesq equation describing the dynamics of two components nerve impulse in the soliton model for biomembranes and nerves. In the last section, the stability of the coupled solitary wave solution is studied both analytically and numerically.

## II. THE COUPLED SOLITARY WAVES MODEL FOR NERVE IMPULSE TRANSMISSION.

The propagation of action potential in the soliton model for biomembranes and nerve is usually considered as a longitudinal compression pulse. This is done by assuming that the diameter of the axon is smaller than the length of the nerve pulse. However, recent studies show that one need not only to consider the longitudinal compressional dislocations but also the out-of-plane transversal mode (i.e., the mode perpendicular to the membrane surface) The propagation of an action potential in the soliton model for biomembranes and nerve is usually considered as a one-dimensional represented by a longitudinal compression pulse; by assuming that the diameter of the axon is smaller than the length of the nerve pulse. However, recent studies show that one need not only to consider the longitudinal compressional dislocations but also the out-of-plane transversal mode (i.e., the mode perpendicular to the membrane surface). By considering the nerve signal  $\mathbf{U}$  as an electromechanical density pulse with two components, the improved Heimburg-Jackson model equation is rewritten as

$$\frac{\partial^2 \mathbf{U}}{\partial t^2} = \frac{\partial}{\partial x} \left\{ \left( c_0^2 + \alpha \mathbf{U} + \beta \mathbf{U} \cdot \mathbf{U} \right) \cdot \frac{\partial \mathbf{U}}{\partial x} \right\} + \nu \frac{\partial^2}{\partial x^2} \left( \frac{\partial \mathbf{U}}{\partial t} \right) - \eta_1 \frac{\partial^4 \mathbf{U}}{\partial x^4} + \eta_2 \frac{\partial^4 \mathbf{U}}{\partial x^2 \partial t^2}. \quad (1)$$

In Eq. (1),  $x$  is the spatial coordinate along the membrane cylinder and  $t$  is time.  $\mathbf{U}$  describes a two component electromechanical density pulse define as

$$\mathbf{U} = u(x, t) \mathbf{e}_r + v(x, t) \mathbf{e}_\theta, \quad (2)$$

where,  $u(x, t)$  and  $v(x, t)$  correspond to the longitudinal and transverse components respectively.  $\mathbf{e}_r$  is the unit vector in the direction of  $u(x, t)$  while  $\mathbf{e}_\theta$  is the unit vector in the direction of  $v(x, t)$ .  $\mathbf{e}_r$  and  $\mathbf{e}_\theta$  satisfy the orthonormal properties  $\mathbf{e}_r \cdot \mathbf{e}_\theta = 0$ ,  $\mathbf{e}_\theta \cdot \mathbf{e}_\theta = 1$ , and  $\mathbf{e}_r \cdot \mathbf{e}_r = 1$ .  $\nu$  is the damping coefficient while  $\eta_2$  and  $\eta_1$  are the dispersion parameters.

The second dispersion coefficient  $\eta_2$  is physically related to the inertia effects of the membrane structure and have been shown to influence the width of the solitary pulse. In this improved model,  $\eta_1$  determines the limiting velocity at high frequencies and  $\eta_2$  governs how this limit is reached [16, 17] and in [19] it was established that  $\eta_2$  increases the stability the nerve signals. A great deal of work has been done on the effects of damping coefficient  $\nu$  on the dynamics of nerve pulse. It has been established that  $\nu$  causes modulation instability in the nerve, and possible generation of localized periodic wave trains [18]. Such localized wave trains were analytically and numerically obtained in [19]. The parameters  $\alpha$  and  $\beta$  describe the nonlinear elastic properties of membranes. At a temperature slightly above the melting transition, the lipid membrane has negative values for the parameter  $\alpha$  and positive values for the parameter  $\beta$

and in low-frequency limit for dipalmitoyl phosphatidylcholine (DPPC) membranes, the initial speed of sound  $c_0 = 176.6$  m/s,  $\alpha = -16.6 \frac{c_0^2}{\rho_0^A}$ , and  $\beta = 79.5 \frac{c_0^2}{(\rho_0^A)^2}$  with initial density of the membrane  $\rho_0^A = 4.035 \times 10^{-3}$  gm $^{-2}$ .

If we assume a small oscillation of the density pulse,  $\mathbf{U} \rightarrow \epsilon \mathbf{U}$  and the system parameters  $c_o \rightarrow \epsilon c_0$ ,  $\eta_2 \rightarrow \epsilon^{-2} \eta_2$ ,  $\nu \rightarrow \epsilon \nu$ , and the transformation

$$y = \epsilon(x - t), \quad s = \epsilon^3 t, \quad (3)$$

$$\frac{\partial u}{\partial s} + \frac{1}{2}(c_0^2 + \beta u^2) \frac{\partial u}{\partial y} - \frac{\eta_1}{2} \frac{\partial^3 u}{\partial y^3} - \eta_2 \frac{\partial^3 u}{\partial y^2 \partial s} - \frac{\mu}{2} \frac{\partial^2 u}{\partial y^2} + \frac{\beta}{2} v^2 \frac{\partial u}{\partial y} = 0, \quad (4)$$

$$\frac{\partial v}{\partial s} + \frac{1}{2}(c_0^2 + \beta v^2) \frac{\partial v}{\partial y} - \frac{\eta_1}{2} \frac{\partial^3 v}{\partial y^3} - \eta_2 \frac{\partial^3 v}{\partial y^2 \partial s} - \frac{\mu}{2} \frac{\partial^2 v}{\partial y^2} + \frac{\beta}{2} u^2 \frac{\partial v}{\partial y} = 0. \quad (5)$$

The nonlinear coupled Burger-KdV-Benjamin-Bona-Mahony equations (4) and (5) describe the dynamics of two coupled solitary waves in the improved soliton model of nerves. It can be used to model the dynamics of the mechanical fields (i.e., relative height field and the lateral stretch field) that has been observed in a neuron. It is instructive to note that, a linearly coupled KdV equations have been used to model two layer settings in various physical systems, such as stratified fluids with a superimposed shear flow, and in dual-core optical waveguides carrying ultrashort pulses. In such a system, two types of vector soliton solutions (i.e., symmetric and asymmetric solitons) are usually obtained using the variation approximation method [31]. In addition, the coupled KdV-Benjamin-Bona-Mahony equation have been used to model the motion of small-amplitude long waves on the surface of an ideal fluid under the gravity force, and in situations where the motion is sensibly two dimensional. In such a system, one of the component models the elevation of the fluid surface from the equilibrium position while the other component models the horizontal velocity in the flow [32].

### III. VARIATIONAL FORMALISM AND ANALYTICAL SOLUTION TO THE COUPLED MODEL EQUATION

The understanding of physical, and, in particular, nonlinear, phenomena through conservation laws and variational formalism is probably the most fundamental and universal approaches to theoretical physics [25]. In this context the natural question is what kind of information can we potentially get from knowing the energy carried by the solitary waves in the nerve fiber?. This approach is widely acknowledged in such branches of nonlinear sci-

ence as fluid dynamics [25, 26], plasma physics [27, 28], and in the recent wave of activity on the dynamics of trapped Bose condensates, as well as in the the general context of the Hamiltonian systems [29]. Here however, we are interested in the solitary wave solution of the coupled system (4) and (5) via variational method. To proceed we first applied traveling wave ansatz method and obtained a set of coupled modified Lienard's equations. It is worth noting that, the modified coupled Lienards equation has been used to model the dynamics of two coupled bursting neurons by considering a set coupled Hindmarsh-Rose (HR) neuron model subjected to an external periodic excitation. Numerical simulations revealed the existence of some bifurcation structures including saddle-nodes, symmetry breaking and period-doubling route to chaos [30]. It is imperative to note that the addition of the frictional term to the classical soliton model gives an additional term to the Lagrangian of the system; the so-called frictional potential term. In order to obtain the Lagrangian density with the damping term, the conventional Lagrangian formalism is inconsistent. Therefore we employed the differential approach which consists of multiplying the conventional Lagrangian with an exponential factor [31, 40–44].

Proceeding as described above, we first seek travelling wave solution of the coupled system (4) and (5) by using the traveling-wave ansatz,  $u = u(y - \xi s) = u(z)$  and  $v = v(y - \xi s) = v(z)$  (where  $\xi$  is the solitary wave velocity). Substituting into Eqs. (4) and (5), we obtained the coupled Lienard's equation

$$\frac{\partial^2 u}{\partial z^2} + \frac{\gamma}{\gamma_o} \frac{\partial u}{\partial z} + \frac{c_o^2 - 2\xi}{2\gamma_o} u + \frac{\beta}{6\gamma_o} u^3 + \frac{\beta}{2\gamma_o} uv^2 = 0, \quad (6)$$

$$\frac{\partial^2 v}{\partial z^2} + \frac{\gamma}{\gamma_o} \frac{\partial v}{\partial z} + \frac{c_o^2 - 2\xi}{2\gamma_o} v + \frac{\beta}{6\gamma_o} v^3 + \frac{\beta}{2\gamma_o} vu^2 = 0, \quad (7)$$

where  $\gamma = \frac{-\nu}{2}$  and  $\gamma_o = \frac{2\xi\eta_2 - \eta_1}{2}$ . In the variational Lagrangian approach, Eqs. (6) and (7) are restated as a variational problem in terms of the Lagrangian  $L'$  given by

$$L' = \left( \frac{1}{2} \{u_z^2 + v_z^2\} - \frac{c_o^2 - 2\xi}{4\gamma_o} \{u^2 + v^2\} \right) e^{\frac{\gamma}{\gamma_o} z} - \left( \frac{\beta}{24\gamma_o} \{u^4 + v^4\} + \frac{\beta}{2\gamma_o} u^2 v^2 \right) e^{\frac{\gamma}{\gamma_o} z}. \quad (8)$$

In Eq. (8), the exponential term  $e^{\frac{\gamma}{\gamma_o} z}$  denotes the damping characteristics of the coupled solitary waves. In order to analyze the dynamics of the coupled solitary waves, we use a reduced variational principle and assume solitary wave ansatz as a trial function. Thus we choose an ansatz of the form

$$(u, v) = (A, B) \text{sech}(az), \quad (9)$$

and substituting this into Eq. (8), we obtain the effective

Lagrangian  $L$ , given by

$$\begin{aligned} L &= \int_{-\infty}^{\infty} L' dz, \quad (10a) \\ &= \left( \frac{3\gamma - 2}{3\gamma} + \frac{3\gamma_o^2(2\xi - c_o^2) - \gamma^2}{6\gamma\gamma_o^2 a^2} \right) (A^2 + B^2) \\ &\quad \times \frac{\gamma\pi}{2\gamma_o} \text{cosec} \left\{ \frac{\gamma\pi}{2\gamma_o a} \right\} \\ &\quad - \frac{\beta}{72\gamma_o^3} \left( \frac{\gamma^2}{a^4} - \frac{4\gamma_o^2}{a^2} \right) (A^4 + B^4 + 12A^2 B^2) \\ &\quad \times \frac{\gamma\pi}{2\gamma_o} \text{cosec} \left\{ \frac{\gamma\pi}{2\gamma_o a} \right\}. \quad (10b) \end{aligned}$$

It should be noted that, the values of the amplitudes  $A$  and  $B$ , and the inverse width  $a$ , for the soliton solutions are real, and can be gotten in terms of the system parameters by using the Euler-Lagrangian equations  $\frac{\partial L}{\partial A} = \frac{\partial L}{\partial B} = \frac{\partial L}{\partial a} = 0$ . Thus, we obtain the system of equations

$$\frac{3\gamma - 2}{3\gamma} + \frac{3\gamma_o^2(2\xi - c_o^2) - \gamma^2}{6\gamma\gamma_o^2 a^2} - \frac{\beta}{36\gamma_o^3} \left\{ \frac{\gamma^2}{a^4} - \frac{4\gamma_o^2}{a^2} \right\} \{A^2 + 6B^2\} = 0, \quad (11a)$$

$$\frac{3\gamma - 2}{3\gamma} + \frac{3\gamma_o^2(2\xi - c_o^2) - \gamma^2}{6\gamma\gamma_o^2 a^2} - \frac{\beta}{36\gamma_o^3} \left\{ \frac{\gamma^2}{a^4} - \frac{4\gamma_o^2}{a^2} \right\} \{B^2 + 6A^2\} = 0, \quad (11b)$$

$$\left( \frac{3\gamma - 2}{3\gamma} + \frac{\gamma^2 - 3\gamma_o^2(2\xi - c_o^2)}{6\gamma\gamma_o^2 a^2} \right) \{A^2 + B^2\} - \frac{\beta}{72\gamma_o^3} \left\{ \frac{3\gamma^2}{a^4} - \frac{4\gamma_o^2}{a^2} \right\} \{A^4 + B^4 + 12A^2 B^2\} = 0. \quad (11c)$$

Note that, in order to obtain Eq. (11c), we assumed a small oscillation in the inverse pulse width  $a$ , such that  $\cot \left\{ \frac{\gamma\pi}{2\gamma_o a} \right\} \approx \frac{2\gamma_o a}{\gamma\pi}$ . Solving simultaneously for  $A$  and  $B$  in Eqs. (11a) and (11b) we obtain

$$(A, B) = \pm \sqrt{\frac{6\gamma_o a^2 (2\gamma_o^2 a^2 \{3\gamma - 2\} + 3\gamma_o \{2\xi - c_o^2\})}{7\beta\gamma \{\gamma^2 - 4\gamma_o^2 a^2\}}}. \quad (12)$$

Substituting Eqs. (12) into Eq. (11c), and solving the resulting equation for  $a^2$ , we obtain two roots given by

$$a^2 = -a_1 + \sqrt{\frac{a_1^2 - 4a_2 a_0}{a_0}}, \quad (13a)$$

$$a^2 = -a_1 - \sqrt{\frac{a_1^2 - 4a_2 a_0}{a_0}}, \quad (13b)$$

where

$$a_o = -8\gamma_o^4(3\gamma - 2), \quad (14a)$$

$$a_1 = -2\gamma_o^2\gamma^2(3\gamma - 2) + 24\gamma_o^4(2\xi - \gamma_o^2) - 4\gamma^2, \quad (14b)$$

$$\text{and } a_2 = 4\gamma^4 - 15\gamma_o^2\gamma^2(2\xi - c_o^2). \quad (14c)$$

Note that the quantity  $a_1 > 0$ , and that  $\sqrt{\frac{a_1^2 - 4a_2 a_0}{a_0}} \ll a_1$ . As a consequence, the two roots of  $a^2$  are approximately equal.

Now let turn to the analysis of the amplitudes  $(A, B)$  of the soliton as depicted by Eq. (12). Since  $(A, B)$  and  $a^2$  must be real for a pulse soliton, then from Eq. (12), it is easy to deduce that  $a^2$  is bounded within the region  $\frac{\nu^2}{4(2\eta_2\xi - \eta_1)} < a^2 < \frac{c_o^2 - 6\xi}{4 + 3\nu}$ . Since  $\nu > 0$ , it follows that the propagation speed  $\xi$  is also bounded in the region  $\frac{\eta_1}{2\eta_2} < \xi < \frac{c_o^2}{6}$ . Figure 1 shows the evolution  $a^2$  against  $\xi$ . In Fig. 1(i), solitary pulse are stable for  $\xi > 800$ , and unstable for  $\xi < 800$  for the given membrane parameters. On the other hand, Fig.1 (ii) and Fig. 1(iii) shows the effect of the inertia parameter  $\eta_2$  and damping parameter  $\nu$  on the stability of the soliton pulse. The plot clearly shows that increasing  $\eta_2$  increases the stability of the soliton pulse while increasing  $\nu$  decreases its stability. As a consequence, stable soliton pulse solutions describe by Eq. (9) is possible if there is a balance between damping and inertia effects of the lipid membrane.

In order to further understand the dynamics of the solutions with respect to the pulse width, we turn our attention to the parameter space plot. First, we find the bifurcation points by setting  $a^2(\eta_2, \xi, \nu) = 0$  and we obtain the fixed points in terms of the parameters  $\eta_2$  and  $\nu$  by solving for  $\xi$ . We then plot the 3D surface  $a_o^2 = F(\eta_2, \nu)$  as a function of two variables  $\eta_2$  and  $\nu$  for

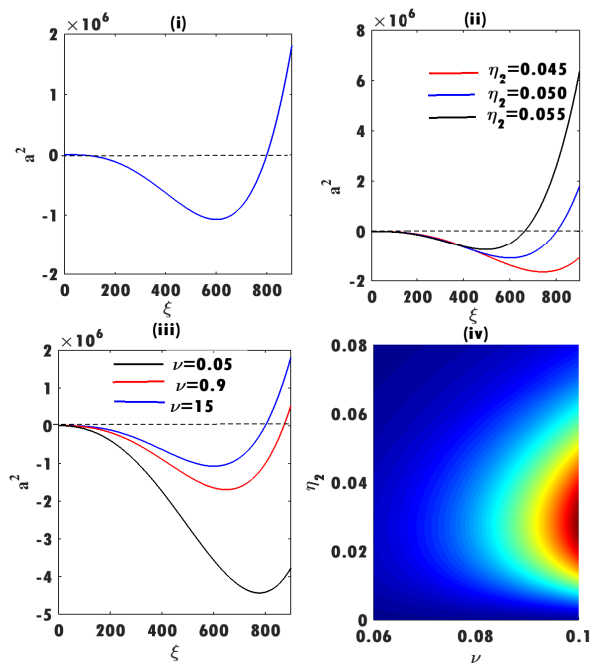


FIG. 1. Evolution of the square of the soliton width as a function of the propagation speed  $\xi$ , as predicted by Eq. (13b). (i) The order parameters are  $\nu = 0.05$ ,  $\eta_1 = 0.05$ ,  $\eta_2 = 0.05$ . For  $a^2 < 0$ , that is complex pulse width (which has no physical significance), Eq. (9) describe periodic solutions for real amplitudes  $A$  and  $B$ . While for  $a^2 > 0$ , that is real pulse width Eq. (9) describe pulse solitons. (ii) The effect of inertia parameter on the dynamics of the soliton. Increasing the inertia parameter leads to an increase in the stability of the soliton pulse. (ii) The effect of damping parameter on the dynamics of the soliton pulse. (iv) The level-zero contour plot of Eq. (13a). The other model parameters are  $\eta_1 = 0.05$ ,  $c_0 = 176.6$ ,  $\rho_0^A = 4.035 \times 10^{-3}$ ,  $\beta = 79.5 \frac{c_0^2}{(\rho_0^A)^2}$ . The level-zero contour depicts all the solution to the equation  $a_0^2 = F(\eta_2, \nu)$  in the contemplated parameter range. Increasing the damping parameter leads to a decrease in the stability of the soliton pulse.

the bifurcation point  $\xi = \xi_0$ . Figure 2(iv) shows the 3D surface  $a_0^2 = F(\eta_2, \nu)$  as introduced in Eq. (13a). This surface depends on two parameters  $\eta_2$  and  $\nu$ . The actual colours of any spot  $(\eta_2, \nu, a_0^2) \in \mathbb{R}^3$  on the surface depends on the height or level of  $a_0^2$  above the  $\eta_2 - \nu$  plane. In this particular graph, the “height” of  $a_0^2$  ranges from 0–10000 in the surface plot.

So far we have analyzed the solutions obtained using the square of the pulse width described by Eq. (13a). If we considered that the amplitudes  $A$  and  $B$  are real functions and that  $a^2 > 0$ , then Eq.(9) is said to describe solitary wave solution which can be symmetric (i.e.,  $A = B$ ) or antisymmetric (i.e.,  $A = -B$ ) [31]. Hence, from Eqs. (12) and Eqs.(9), the two-component soliton model admits three possible types of solutions: dark-dark, bright-bright, and bright-dark solitary wave solutions. The bright-dark solitary wave solution correspond to the an-

tisymmetric case while the dark-dark, and bright-bright solitary wave solutions corresponds to the symmetric case. It should noted here that the bright-dark mode has been recorded experimentally in the garfish olfactory nerve, squid giant axon, and hippocampal neuron [1–4, 21].

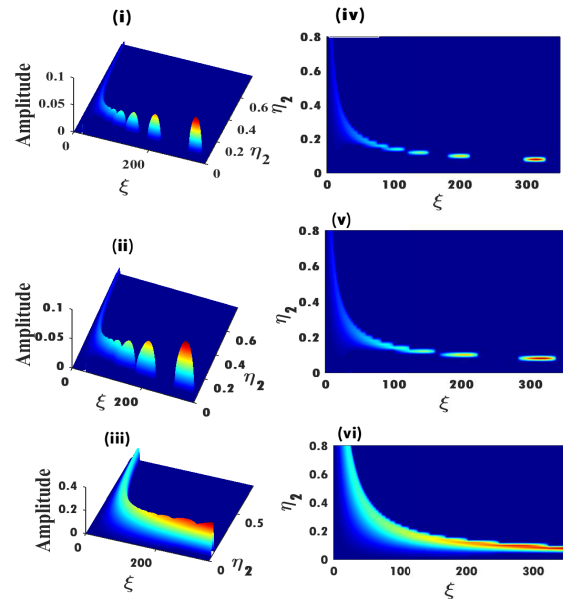


FIG. 2. The evolution of soliton amplitude with propagation speed  $\xi$  and initial parameter  $\eta_2$  for different values of the damping coefficient  $\nu$  and their corresponding contour plot in the  $\eta_2 - \xi$  space of Eq. (12): (i)-(iv)  $\nu = 0.05$ , (ii)-(v)  $\nu = 0.08$  and (iii)-(vi)  $\nu = 0.5$ . The other model parameters are  $\rho_0^A = 4.035 \times 10^{-3}$ ,  $\beta = 79.5 \frac{c_0^2}{(\rho_0^A)^2}$ . The amplitude response as a function of the propagation speed and the initial parameter shown the threshold and saturation effect. The evolution of amplitude as a function of damping parameter  $\nu$  show the effect of discontinuity in the propagation speed.

Now consider the behavior of the soliton amplitudes with the parameters of the system. Analysis of the soliton amplitudes can be used to predict nonlinear phenomenon such as symmetry breaking or discontinuity. It should be noted that in [31], symmetry breaking in a linearly coupled Korteweg-de Vries system was observed. It was shown that the linear KdV equation exhibit symmetry breaking depending on the propagation velocity. Also in Ref. [33], the authors investigated numerically the existence, and stability of solitons in parity-time-symmetric optical media characterized by a generic complex hyperbolic refractive index distribution and fourth-order diffraction. They showed that the fourth-order diffraction coefficient greatly alters parity-time-breaking points. In lipid membrane, discontinuity or non-linearity in state diagram has been studied both theoretically and experimentally [1–5, 34], and it is thought to results from the liquid-expanded-liquid condensed phase change in lipid monolayers. In fact, it is reported that the velocity of

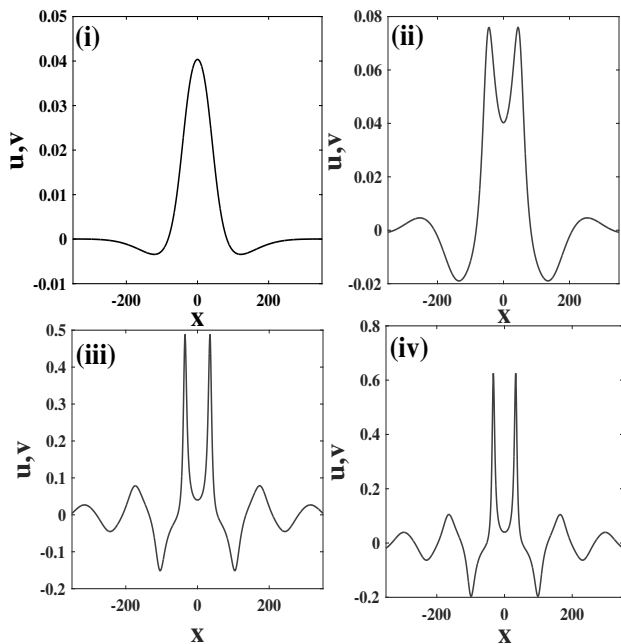


FIG. 3. The evolution of pulse shape as a function of propagation speed  $\xi$  within one of the one of stable island describe in figure 4(iv): (i)  $\xi = 165.8$ , (ii)  $\xi = 165.5$ , (iii)  $\xi = 165.0$  and  $\xi = 164.9$ . The other model parameters are  $\epsilon = 0.001$ ,  $t = 0$ ,  $\eta_1 = 0.045$ ,  $\nu = 0.05$ ,  $\rho_0^A = 4.035 \times 10^{-3}$  and  $\beta = 79.5 \frac{c_0^2}{(\rho_0^A)^2}$ . The solitary wave evolve into a solitary oscillatory shock-like waves as the propagation speed is gradually reduced. Waves with smaller propagation speed turns to propagates with higher amplitudes.

sound decreases discontinuity as the system goes from LE phase to LE-LC coexistence phase in liquid monolayers. Figures 3 (iv) and 3 (v) exhibits in parameter space  $(\eta_2, \xi)$  the stable and unstable regions. One observes the discontinuity of the stable region, which appear like the island of points when the damping parameter is varied. It should be noted that discontinuity in speed implies a discontinuity in the compressibility. Discontinuity in biomembranes indicates an abrupt-phase transition, and near phase transitions, stable solitary waves can propagate along the nerve fiber. In order to investigate stable solitary waves near the region of discontinuity, we plotted the soliton profile within the stable region in Fig.3 (iv) for different values of the propagation speed (see Fig.3). It is worth noting that as the speed of the wave is gradually reduce, the single pulse created evolved into an oscillatory solitary shock-like wave. Figure 2 (vi), exhibits continuity in the stable region within the parameter space  $(\eta_2, \xi)$  resulting from an increase in the damping coefficient. In Refs. [34, 35], Shrivastava *et al.* have recently found that a two-dimensional solitary shock wave reminiscent of propagating spikes in nerves can be induced in monolayer lipid membrane near a phase transition. These waves have a threshold for excitation and an up-

per bound on the maximum amplitude (all-or-none) and are self-sustaining. In [35], Shrivastava further proposed that the observed solitary shock waves at lipid interface also provide evidence for the detonation of shock waves at such interfaces. That is, the self-sustaining shock wave utilizes the latent heat of phase transition of the lipids (i.e., chemical energy stored in lipids interface) reinforcing it in the process. One needs to stress here that the general form of the nonlinear evolution we have considered allows for other possible sources of chemical energy that can reinforce the propagating shock wave. Furthermore, shock waves have been reported to be signature for traumatic brain injury [36]. It is well known that exposure of biological cells to shock waves causes damage to the cell membrane, however, the mechanisms by which damage is caused and how it depends on physical parameters of the shock waves such as shock waves velocity, shock waves duration, shock waves shape, and amplitudes is poorly understood. Figure 5 shows generation of solitary shock-like waves at particular propagation velocity, with different amplitudes and shock waves profiles. Sliozberg *et al.* demonstrated numerically using coarse-grained model of lipids vesicle the principle of damage induced by shock waves by direct passage through the cranium. The results show that the structural integrity of the lipid vesicles is altered as pores are formed in the lipid membrane. As a result, the membrane becomes permeable to sodium, potassium and calcium ions and therefore a possible source of chemical energy for the shock waves [36]. It should be stressed that, a number of scientists have shown that membranes can display ion channel-like current traces even in the complete absence of proteins provided only that the membrane is close to a melting transition [37–39]. These events are called “lipid channels” and consists of small pores or defects in the lipid membranes. We proposed that the observed solitary shock-like wave in the coupled-model in might be responsible for the defects in the lipid membrane near phase transitions.

Consider the interaction of the two coupled solitary waves. From Eqs. (8), (9), and (10a), and noting that  $A^2 = B^2$ , we obtain the effective potential energy function  $U_s$  of the coupled solitary waves

$$U_s = \frac{\gamma_o^2 \gamma \pi (c_o^2 - 2\xi) + \gamma^3 \pi}{2\gamma \gamma_o^3 a^2} \operatorname{cosec} \left\{ \frac{\gamma \pi}{2\gamma_o a} \right\} A^2 + \frac{\beta \pi \gamma}{72 \gamma_o^4} \left\{ \frac{\gamma^2}{a^4} - \frac{4\gamma_o^2}{a^2} \right\} \operatorname{cosec} \left\{ \frac{\gamma \pi}{2\gamma_o a} \right\} A^4. \quad (15)$$

In order to conveniently analyze the characteristic of energy function, we plot the curve of  $U_s$  against  $\xi$ . In view of Fig. 4,  $U_s$  is positive in modeling region and therefore the potential function of interaction is always negative. Thus, the interaction between the two solitary waves is attractive; this agrees with the fact of neural coupling oscillation.

In this section, we analyzed the characteristics of two coupled solitary waves in nerve impulse transmission. We employ an approximate approach using the variational

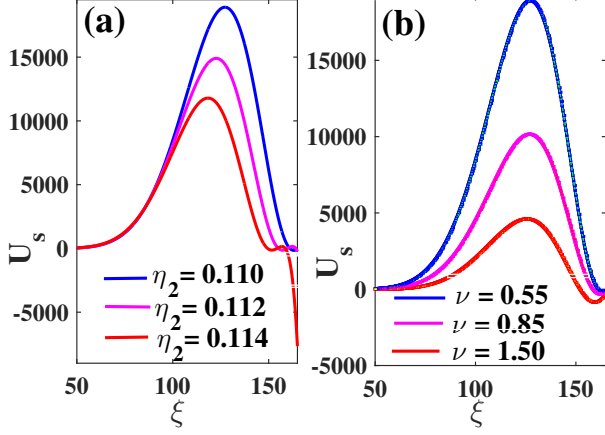


FIG. 4. The energy of the two solitary waves  $U_s$  as a function of propagation speed  $\xi$ . (a) The effect of the inertia parameter  $\eta_2$  for  $\nu = 0.55$ . (b) The effect of the damping parameter  $\nu$  for  $\eta_2 = 0.110$ . The energy of the two solitary waves decrease as the damping coefficient and inertia coefficient increases. The other model parameters are  $\eta_1 = 0.045$ ,  $c_0 = 176.6$ ,  $\rho_0^A = 4.035 \times 10^{-3}$  and  $\beta = 79.5 \frac{c_0^2}{(\rho_0^A)^2}$ .

principle and obtained a solution for the coupled solitary wave within the framework of the soliton model described by coupled KdV-BBM equations in the presence of damping. We showed that, a small friction potential present in the coupled solitary wave model induced discontinuity (or phase transitions) in the amplitude (density change)-velocity parameter space, a reminiscent for propagation of solitary shock-waves and a single soliton pulse. The relevant biological implication is also discussed. In the next section we will study linear stability analysis of the solitary waves solution obtained in this section.

#### IV. LINEAR STABILITY ANALYSIS

In non-linear waves, solitons and their linear stability properties are crucial. In integrable systems, solitons admit analytical expressions and they are generally stable against small perturbations. In non-integrable systems, solitons generally do not admit analytical expressions and can be either stable or unstable. The understanding of many properties of these nonlinear waves can be achieved through the calculation of their spectra. Indeed, spectral analysis of the equations appearing after linearization of the governing non-linear equations near, the solitons has become widespread tools. Bound eigenstates, which do not grow with propagation or in time, of the linear problem, are often called internal modes. Internal modes supported by the single mode soliton in the soliton model of nerve has been studied in [19]. In this section, we compute the linear-stability spectrum of the solitary wave obtained; which consists of eigenvalues of the linear-stability operator of the solitary wave [48]. The linear-stability spectrum contains valuable information on the solitary wave. For instance, if this spectrum contains eigenvalues with positive real parts, then the solitary wave is linearly unstable. In this case, the largest real part of the eigenvalues gives the maximal growth rate of perturbations. If the spectrum contains purely imaginary discrete eigenvalues, these eigenvalues are the internal modes [48, 49]. In particular, persistent oscillations of the soliton width and position are due to these modes.

To proceed, we consider a small perturbation in  $u$  and  $v$  given by  $u = u_0 + \varphi u_1$  and  $v = v_0 + \varphi v_1$  where  $\varphi \ll 1$  and  $u_0$  and  $v_0$  is the solution to the Eqs. (4) and (5) given by Eq. (9). Substituting  $u = u_0 + \varphi u_1$  and  $v = v_0 + \varphi v_1$  into Eqs. (4) and (5) and linearising about  $\varphi$  the linearise system

$$\frac{\partial u_1}{\partial s} + \frac{1}{2} \{c_0^2 + \beta(u_0^2 + v_0^2)\} \frac{\partial u_1}{\partial y} + \beta(u_0 u_1 + v_0 v_1) \frac{\partial u_0}{\partial y} - \frac{\eta_1}{2} \frac{\partial^3 u_1}{\partial y^3} - \eta_2 \frac{\partial^3 u_1}{\partial y^2 \partial s} - \frac{\nu}{2} \frac{\partial^2 u_1}{\partial y^2} = 0, \quad (16a)$$

$$\frac{\partial v_1}{\partial s} + \frac{1}{2} \{c_0^2 + \beta(u_0^2 + v_0^2)\} \frac{\partial v_1}{\partial y} + \beta(u_0 u_1 + v_0 v_1) \frac{\partial v_0}{\partial y} - \frac{\eta_1}{2} \frac{\partial^3 v_1}{\partial y^3} - \eta_2 \frac{\partial^3 v_1}{\partial y^2 \partial s} - \frac{\nu}{2} \frac{\partial^2 v_1}{\partial y^2} = 0. \quad (16b)$$

Since the linearisation is near a solitary wave, i.e, Eq. (9), then Eqs. (16a) and (16b), reduces into an eigenvalue

problem:

$$Q\mathbf{V} = \lambda\mathbf{V}. \quad (17)$$

In Eq. (17),  $\mathbf{V}(\mathbf{y}) = (u_1, v_1)^T$  is the eigenfunction,  $\mathbf{y} = (y_1, \dots, y_N)$ , where  $N$  is the number of spatial dimensions.  $\lambda$  is the eigenvalue while  $Q$  is the linearization operator (usually non-Hermitian) and is given by

$$Q = \frac{1}{2} \begin{pmatrix} (1 - \eta_2 \partial_y^2)^{-1} (G_1 \partial_y - \eta_1 \partial_y^3 - \nu \partial_y^2 + G_0) & (\eta_2 \partial_y^2 - 1)^{-1} G_2 \\ (\eta_2 \partial_y^2 - 1)^{-1} G_2 & (1 - \eta_2 \partial_y^2)^{-1} (G_1 \partial_y - \eta_1 \partial_y^3 - \nu \partial_y^2 + G_0) \end{pmatrix} \quad (18)$$

$$\begin{cases} G_0 = -2\beta A^2 \operatorname{sech}^2(ay)\tanh(ay), \\ G_1 = c_0^2 + 2\beta A^2 \operatorname{sech}^2(ay), \\ G_2 = 2aA^2 \operatorname{sech}^2(ay)\tanh(ay). \end{cases} \quad (19)$$

The continuous spectrum of the system is determined analytically by examining the matrix  $Q$  as  $\mathbf{y} \rightarrow \infty$ . Proceeding with this approximation, it is easy to show that the continuous eigenvalues are

$$\lambda = \pm \frac{1}{2} \left\{ i \frac{c_0^2 k + \eta_1 k^3}{1 + \eta_2 k^2} + \frac{\nu k^2}{1 + \eta_2 k^2} \right\}. \quad (20)$$

where  $k$  is the perturbation wave number. Discrete eigenvalues do exist, however, they can only be obtained numerically. The local growth rate of the solitons or the gain is given by  $\operatorname{Im}(\lambda)$ . The maximum growth rate of the soliton can be obtained by solving the equation  $\frac{d\operatorname{Im}(\lambda)}{dk} = 0$ . Applying this definition, it is easy to show that,

$$k_{\pm}^2 = \frac{\eta_2 c_0^2 - 3\eta_1 \pm \sqrt{(3\eta_1 - \eta_2 c_0^2)^2 - 4\eta_1 \eta_2 c_0^2}}{2\eta_1 \eta_2}. \quad (21)$$

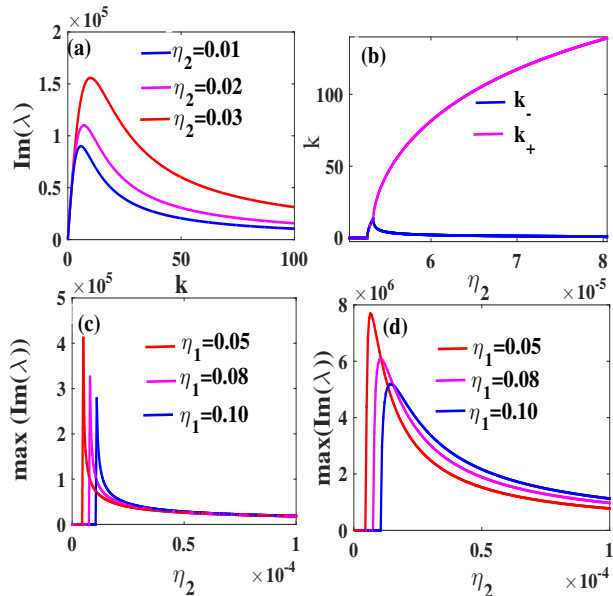


FIG. 5. (a) The perturbation growth rate of solitons versus  $k$  with different values of  $\eta_2$ ,  $\eta_1 = 0.05$  (b) Bifurcation diagram of soliton states in the two components model.  $0 < \eta_2 < 5.32 \times 10^{-5}$ , the wave number  $k = 0$ ,  $k = 5.1 \times 10^{-5}$ , there is a growth in the wave number  $k$  and at  $k = 5.32 \times 10^{-5}$ , the soliton split into two soliton states with wave number  $k_-$  and  $k_+$ . Note that their antisymmetric components  $-k_-$  and  $-k_+$  are not shown on the diagram and  $\eta_1 = 0.55$  (c) and (d) corresponds to the maximum perturbation growth rate of solitons states  $k_-$  and  $k_+$  respectively versus  $\eta_2$  with different values of  $\eta_1$ . The order parameter  $c_0 = 176.6$ .

The stability of the perturbed soliton  $u, v$  is related to the imaginary parts  $\operatorname{Im}(\lambda)$  of all eigenvalues  $\lambda$ . If

$|\operatorname{Im}(\lambda)| > 0$ , then the solution  $(u, v)$  will grow exponentially with  $y$  (i.e., it is unstable), otherwise, the solution  $(u, v)$  is stable. In the existence range of the approximation described above, the dependence of the perturbation growth rate (the most unstable growth rate) on the parameter  $\eta_1$  and  $\eta_2$  are exhibited Fig. 5 (a) and 5(c-d) respectively. As it can clearly be observed,  $\eta_1$  and  $\eta_2$  reduces the instability growth rate of the solitons.

In order to confirm the stability or instability of the system, one needs to solve the eigenvalue equation (17) numerically. One of the methods used to solved such a problem is the finite difference discretizations method. However, the accuracy of this method is quite low. In addition, this method has been reported to give spurious eigenfunction even when the eigenvalues obtain are approximately correct. A more accurate method is the Fourier collocation method (FCM) [48]. By this method, the eigenfunction  $\mathbf{V}$  is expanded into a Fourier series and Eq. (17) is turned into a matrix eigenvalue problem for the Fourier coefficients of the eigenfunction  $\mathbf{V}$ . The structure of the resulting matrix depends heavily on the structure of the spatial dimension of Eqs. (4) and (5). A detail analysis of the Fourier collection method can be found in [48–50]. The results from the numerical simulation is illustrated in Fig. (6).

Figure 6 (a1, b1, c1) illustrate the unperturbed soliton profiles for different values of the propagation speed  $\xi$  used in our numerical simulation while Fig. 6 (a2, b2, c3) corresponds to the numerically computed eigenvalue spectrum. As can clearly seen, Fig. 6 (a2) describe a bound state or internal mode. In particular, persistent oscillations of the soliton width, and position are due to these modes. On the other hand, Fig. 6 (a3) illustrate to the stable propagation of the perturbed solution while Fig. 6 (b3, c3) illustrate unstable propagation of the intensity of the perturb solution.

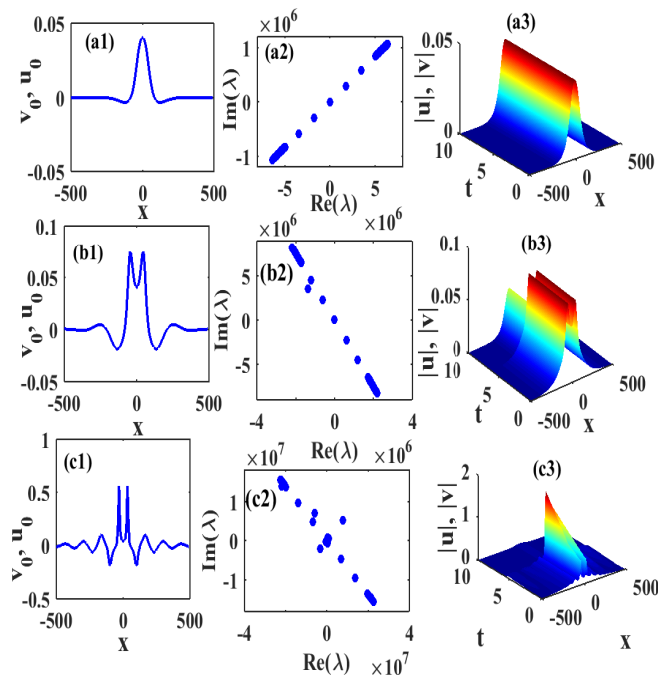


FIG. 6. (a1, b1, c1) Initial solitary wave profile as given by Eq. (9). (a2, b2, c2) Numerically computed linear stability spectra. (a3) Stable and (b2, c3) unstable propagations of perturbed solution  $u = u_0 + \varphi u_1$  and  $v = v_0 + \varphi v_1$ . (a1, a2, a3)  $\xi = 165.8$ , (b1, b2, b3)  $\xi = 165.5$ , and (c1, c2, c3)  $\xi = 165.0$ . The other model parameters are  $\epsilon = 0.001$ ,  $\eta_1 = 0.045$ ,  $\nu = 0.05$ ,  $\rho_0^A = 4.035 \times 10^{-3}$ ,  $\varphi = 10^{-33}$ ,  $\eta_2 = 0.11$ , and  $\beta = 79.5 \frac{c_0^2}{(\rho_0^A)^2}$ .

## V. DISCUSSION AND CONCLUSION

Electromechanical solitary wave measurements on nerve fibers began in the early 1980s with the measuring of various non-electrical components of action potential and the investigation of the chemistry of phase transitions in nerve fibers, and its importance for nerve pulse propagation by Tasaki [51] and by Kaufmann proposal of sound waves as a physical basis for action potential propagation in the nerve. This mechanical aspect of action potential gained more attention when Heimburg and Jackson proposed the soliton model for nerve pulse propagation in the early 2000s [4]. Since that time, the dynamics of a pulse, propagation has been extensively stud-

ied by a wide variety of applied scientists; and, partly as a result of recent interest shown by applied mathematicians in the nonlinear diffusion equation, single dynamics is now a rather well understood physical phenomenon [13–19]. One might suppose that this is the end of the story; on the contrary, it is only the beginning. Recent studies have shown that the electromechanical density pulses in the nerve can effectively be considered as a vector soliton with two components. That is, the longitudinal component corresponding relative height field and the transverse components corresponding to the lateral stretch field and have been observed experimentally in garfish olfactory nerve, squid giant axon, and hippocampal neuron [21].

In this work, we have considered the electromechanical density pulse as a two coupled solitary waves represented by longitudinal compression wave and an out-of-plane transversal pulse (i.e., perpendicular to the membrane surface) and analyzed using the variational approach the characteristics of the coupled solitary waves in the presence of damping within the framework of coupled nonlinear Burger-Korteweg-de Vries-Benjamin-Bona-Mahony equations (BKdV-BBM) derived from the vector soliton model equation for biomembranes and nerves. In particular, we have shown that, there must be a balanced between damping and inertia effects for a stable coupled solitary waves to propagate within the axon. Furthermore, we have shown that the presence of damping coefficient causes a discontinuity in the  $(\eta_2, \xi)$  parameter space. In particular, we observed a discontinuity in stable regions stable region which appears like the island of points. Analysis of the solitary wave energy shows that both  $\eta_2$  and  $\nu$  causes a decrease the energy of the coupled solitary waves. In addition, the potential function of interaction is shown to be always negative. Thus, the interaction between the two solitary waves is attractive; which is agreement with the fact of neural coupling oscillation. We performed linear stability analysis and the results shows that both  $\eta_2$  and  $\nu$  decreases the perturbation growth rate of the coupled solitary waves. Numerical simulation of the linearized equation shows that the bell shape solitary wave profile yields a bound eigenvalue spectrum while the solitary shock-like solitary waves produce an unbound eigenvalue spectrum. Thus the bell shape profile is generally stable for a small perturbation while the solitary-shock like profile is generally unstable. The instability of these shock-like solitary waves might be responsible for traumatic brain injury and damage to the cell membrane [36].

[1] J. Griesbauer, S. Bossinger, A. Wixforth, and M. Schneider, *Phys. Rev. Lett.* **108**, 198103 (2012).  
 [2] J. Griesbauer, M. F. Schneider, *Biophys. J.* **97**, 2710 (2009).  
 [3] J. Griesbauer, S. Bossinger, A. Wixforth, and M. Schneider, *Phys. Rev. E* **86**, 061909 (2012).

[4] T. Heimburg and A. D. Jackson, *PNAS* **102** 9790 (2005).  
 [5] S. S. L. Andersen, A. D. Jackson and T. Heimburg, *Prog. Neurobiol.* **88** 104 (2009).  
 [6] A. L. Hodgkin and A. F. Huxley, *J. Physiol. London* **117**, 500(1952).  
 [7] A. L. Hodgkin and A. F. Huxley, *J. Physiol.* **104**, 176

- (1945).
- [8] A. L. Hodgkin, A.F. Huxley, and B. Katz, *J. Physiol.* **116**, 424(1952).
- [9] E. Neher and B. Sakmann, *Nature* **260**, 799 (1976).
- [10] A. D. Doyle, J. M. Pfuetzner, A. Kuo, S. L. Cohen, B. T. Chait, and R. Mackinnon, *Science*, **280**, 69 (1998).
- [11] G. H. Kim, P. Korstein, L. Obeid, and B. M. Salzberg, *Biophys. J.* **92**, 3122(2007).
- [12] S. Shrivastava and M. F. Schneider, *J. R. Soc. Interface* **11**, 0098 (2014).
- [13] F. Contreras, F. Ongay, O. Pavon, and M. Aguero, *Int. J. Mod. Nonlin. Theory Appl.* **2**, 7 (2013).
- [14] F. Contreras, H. Cervantes, M. Aguero, and Ma. de L. Najera, *J. Nonlin. Dyn.* **2014**, 710152 (2014)
- [15] E. V. Vargas, A. Ludu, R. Hustert, Peter Gumrich, A. D. Jackson, and Thomas Heimburg, *Biophys. Chem.* **153**, 159 (2011).
- [16] J. Engelbrecht, T. Peets, K. Tamm, M. Laasmaa, and M. Vendelin, *Proc. Estonian Academy of Sciences* **67**, 28 (2018)
- [17] J. Engelbrecht, K. Tamm, and T. Peets, *Biomech. Chem. Phys. Med. NMR* **14**, 159 (2015).
- [18] G. Fongang Achu, F. M. Moukam Kakmeni, and A. M. Dikande, *Phy. Rev. E* **97**, 012211 (2018).
- [19] G. Fongang Achu, S. E. Mkam Tchouobiap, F. M. Moukam Kakmeni, and C. Tchawoua, *Phy. Rev.* **98**, 022216 (2018).
- [20] V. Vogel and D. Möbius, *Langmuir* **1989**, 129 (1988).
- [21] A. E. Hady and B. B. Machta, *Nat. Commun.* **6**, 6697 (2005).
- [22] W. M. Grill, S.E. Norman, and R. V. Bellamkonda, *Annu. Rev. Biomed. Eng.* **11**,1(2009).
- [23] L. Tonello and M. Cocchi, *NeuroQuantology* **8**, 1 (2010).
- [24] J. Engelbrecht, K. Tamm, and T. Peets, *Biomech. Model. Mechanobiol.* **14**, 159 (2015).
- [25] P. J. Morrison, *Rev. Mod. Phys.* **70**, 467(1998).
- [26] R. S. MacKay and P. G. Saffman, *Proc. R. Soc. London, Ser. A* **406**, 115 (1986).
- [27] A. Hasegawa, *Plasma Instabilities and Nonlinear Effects* (Springer-Verlag, Berlin, 1975)
- [28] A. J. Brizard, J. J. Morehead, and A. N. Kaufman, *Phys. Rev. Lett.* **77**, 1500 (1996).
- [29] D. L. Feder, A. A. Svidzinsky, A. L. Fetter, and C. W. Clark, *Phys. Rev. Lett.* **86**, 564 (2001).
- [30] E. M. Yamakou, E. M. Inack, and F. M. Moukam Kakmeni, *Nonlin. Dyn.* **83**, 541 (2015).
- [31] A. Espinosa-Ceron, B. A. Malomed, J. Fujioka, and R. F. Rodriguez, *CHAOS* **22**, 033145 (2012).
- [32] J. L. Bona, M. Chen, and J. C. Saut, *J. Nonlinear Sci.* **12**, 283 (2002).
- [33] C. G. L. Tiofack, F. Ndezana, A. Mohamadou, and T. C. Kofane, *Phys. Rev. E.* **97**, 032204(2018)
- [34] S. Shrivastava, K. H. kang, and M. F. Schneider, *Phys. Rev. E* **91**, 012715(2015)
- [35] S. Shrivastava, *Proc. Mtgs. Acoust.* **34**, 045034 (2018)
- [36] Y. Sliozberg and T. Chantawansri, *J. Chem. Phys.* **141**, 184904 (2014).
- [37] A. Blicher, K. Wodzinska, M. Fidorra, M. Winterhalter, and T. Heimburg, *Biophys. J.* **96**, 4581(2009).
- [38] K. R. Laub, K. Witschas, A. Blicher, S. B. Madsen, A. Luckhoff, and T. Heimburg, *Biochim. Biophys. Acta* **1818**, 1123 (2012).
- [39] A. Blicher and T. Heimburg, *PloS One* **8**, e65707 (2013).
- [40] D. Anderson, *Phys. Rev. A* **27**, 3135 (1983).
- [41] G. Iooss and D. D. Joseph, *Elementary stability and Bifurcation Theory* (Springer, New York, 1980).
- [42] D. Schuch, *J. Phys.: Conf. Ser.* **380**, 20120(2012)
- [43] P. Caldirola, *Nuovo Cimento* **18**, 393 (1941)
- [44] E. Kanai, *Progr. Theor. Phys.* **3**, 537 (1948).
- [45] F. G. Mertens, N. R. Quintero, and A. R. Bishop, *Phys. Rev. E* **81**, 016608 (2010).
- [46] F. G. Mertens, N. R. Quintero, I. V. Barashenkov, and A. R. Bishop, *Phys. Rev. E* **84**, 026614 (2011)
- [47] N. R. Quintero, F. G. Mertens, and A. R. Bishop, *Phys. Rev. E* **91**, 012905 (2015)
- [48] J. Yang, *Nonlinear Waves in Integrable and Nonintegrable Systems* (Society for Industrial and Applied Mathematics, Philadelphia, USA, 2010)
- [49] D. Gottlieb and S.A. Orszag, *Numerical Analysis of Spectral Methods: Theory and Applications* (Society for Industrial and Applied Mathematics, Philadelphia, USA, 1977).
- [50] M. Grillakis, *Comm. Pure Appl. Math.* **41**, 747(1988)
- [51] I. Tasaki, *Physiol. Chem. Phys. Med. NMR* **20**, 251(1988).